A new waveform analysis technique to extract good energy and position resolution from a dual-axis duo-lateral position-sensitive detector

M.W. Aslin[a,b], A. Hannaman[a,c,*], M.D. Youngs[a], A.B. McIntosh[a], A. Abbott[a,c], P. Adamson[a,d], J. Gauthier[a], K. Hagel[a], A. Jedele[a,c], Y.-W. Lui[a], L.A. McIntosh[a], M.Q. Sorensen[a,c], Z.N. Tobin[a,c], R. Wada[a], A. Wakhle[a], S.J. Yennello[a,c]

[a] *Cyclotron Institute, Texas A&M University, College Station, TX 77843, USA*
[b] *Mount Holyoke College, South Hadley, MA 01075, USA*
[c] *Chemistry Department, Texas A&M University, College Station, TX 77843, USA*
[d] *Angelo State University, San Angelo, TX 76909, USA*

Abstract

The dual-axis duo-lateral position-sensitive silicon detector was developed to detect charged particles with high quality position and energy resolution. When these detectors were used with conventional signal processing electronics, an empirically determined correction was used to improve energy resolution. In this work, the waveforms from the detector after preamplification are studied in detail to investigate position information contained in the waveforms. A 7.22 MeV/nucleon alpha particle beam was impinged directly on a masked dual-axis duo-lateral detector. Data obtained using a ^{228}Th alpha particle source was also used. By studying the waveform characteristics that give rise to the position-dependent distortions, a new summed trigger analysis method has been developed to significantly improve linearity in position reconstruction without sacrificing energy resolution.

Keywords: Silicon, Position-sensitive, Charged particle

1. Introduction

Mechanistic studies of heavy-ion reactions require precise measurements of the position and energy of reaction products. Typically, position information is achieved by using a large number of individual detectors [1, 2] or highly segmented double sided strip detectors [3, 4]. In these cases, the angular granularity of the array is dictated by the number of detectors or strips, which adds complexity and cost due to the number of electronics channels. Alternatively, resistive position sensitive silicon detectors can provide excellent position and energy resolution while reducing the required number of channels of electronics. To this end, the Forward Array Using Silicon Technology (FAUST) implements dual-axis duo-lateral (DADL)

*Corresponding Author
Email address: andyhannaman@tamu.edu (A. Hannaman)

position-sensitive detectors to provide the position resolution necessary for such studies [5]. Though a DADL has only four signals, it can still deliver position resolution analogous to that achieved by a 100 by 100 double sided strip detector of a similar size [6]. Further, the position and energy determination in principle only requires simple algebra, making its relative simplicity ideal for complex multidetector arrays [7]. Previous experiments using a DADL detector have shown non-linearities in position and energy reconstruction [5]. This work presents the results of an investigation into the position dependence of the signal shape collected by the DADL detector and presents a new waveform analysis method that cleanly compensates for these distortions without sacrificing energy resolution.

2. Dual-axis duo-lateral position-sensitive detectors

The DADL detectors are nominally 300 µm thick silicon diodes fabricated by Micron Semiconductor, each with an active area of 20 mm x 20 mm[8]. Figure 1 illustrates the geometry and key features of the detector. The electrode on the front face is resistive with contacts at the bottom (F1) and top (F2) for position measurement in the vertical direction, while the electrode on the back face is resistive with contacts at the left (B1) and right (B2) for position measurement in the horizontal direction. Negative voltage is applied to the front (p-type side) to reverse-bias the detector. When ionizing radiation excites electrons from the valence band to the conduction band, the bias attracts the holes to the front electrode and the electrons to the back electrode. Once on the face, the charge carriers split between the two contacts. Conductive strips (equipotential lines in Figure 1) embedded in the resistive electrode allow the charge carriers to spread out to facilitate collection of all the charge at the appropriate electrodes. To prevent charge bleeding, conductive guard rings surround the electrodes as shown in Figure 1. The fraction of the charge collected on a given electrode (e.g. F1) is directly proportional to the distance between the opposite electrode (F2) and the origin of the liberated charge. Local position coordinates X and Y can therefore be calculated from the charges Q_{Bottom}, Q_{Top}, Q_{Left} and Q_{Right} according to Equations 1 and 2 corresponding to the contacts F1, F2, B1, and B2 respectively. Scaling parameters c_{x} and c_{y} are included to ensure the apparent size of each detector according to the measurement matches the physical size of the detector.

$$X = c_x * \frac{Q_{\mathrm{Right}} - Q_{\mathrm{Left}}}{Q_{\mathrm{Right}} + Q_{\mathrm{Left}}} \tag{1}$$

$$Y = c_y * \frac{Q_{\mathrm{Top}} - Q_{\mathrm{Bottom}}}{Q_{\mathrm{Top}} + Q_{\mathrm{Bottom}}} \tag{2}$$

The charge collected on each face is proportional to the energy deposited by a particle. For the DADL detector, the charge collected by both contacts of a face is summed together in order to determine E_{F} and E_{B} as shown in Equations 3, 4, 5. Two different methods are used in this paper to determine a representation of the charge collected by a contact and are described in Section 4.

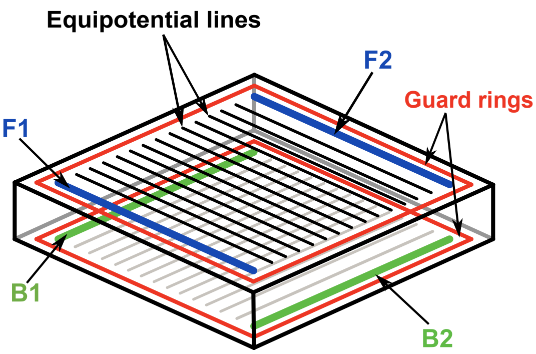

Figure 1: Schematic diagram of a DADL detector. Four contacts collect charge, indicated by F1 and F2 on the front face, and B1 and B2 on the back face. Equipotential conductive lines facilitate lateral charge movement to the contacts. Guard rings on both faces of the detector prevent minor position distortions and charge bleeding [6]. Thickness and area are not drawn to scale.

$$E = E_{\mathrm{F}} = E_{\mathrm{B}} \tag{3}$$

$$E_F \propto Q_{\mathrm{Bottom}} + Q_{\mathrm{Top}} \tag{4}$$

$$E_B \propto Q_{\mathrm{Left}} + Q_{\mathrm{Right}} \tag{5}$$

3. Experimental Setup

Tests of the performance characteristics of a DADL detector were conducted at the Texas A&M University Cyclotron Institute using beams from the TAMU K150 Cyclotron. A beam of 7.22 MeV/nucleon alpha particles was impinged on a DADL detector. Additional tests were performed using a ^{228}Th alpha source placed 10 cm in front of the detector. The DADL detector was reverse-biased by applying -40 V to the front face of the detector (both F1 and F2) and grounding the back face (B1 and B2) using 50 Ω terminators. The front guard ring was biased at -36.4 V using a resistive voltage divider, and a 50 Ω terminator was used to hold the back guard ring at ground.

The signals from each of the four contacts were sent to a RisCorp 110 mV/MeV charge-sensitive preamplifier, the output of which was connected to the input of a Struck SIS3316 waveform digitizer. Waveforms were recorded using 4 ns wide bins for a length of 32 µs beginning around 3 µs before an internal trigger. Each waveform, denoted by the name of the contact from which it was collected, was then analyzed offline. This differs from previous work which employed the HINP ASIC shaping amplifiers and a peak-sensing ADC housed in an XLM-XXV rather than the SIS3316 [9, 10, 5]. A physical mask made of 0.25 inch-thick brass plate was fashioned with precision slits and holes. For some of the data collection, this mask was placed 0.5 inches from the detector to block incident charged particles. This allows assessment of position resolution as well as position dependence of the apparent measured energy. The details of the mask are discussed below (see Figure 4).

4. Analysis and Results

Waveforms of the preamplifier output were recorded to study the origin of distortions previously observed using the shaping electronics method [10]. For each waveform, an average baseline value was calculated over the first 100 bins (400 ns) and subtracted from the total waveform. The full 32 µs lengths of the baseline-corrected waveforms from a single event are shown in Figure 2(a). Some waveforms in this plot, most clearly seen in waveforms F1 and B2, are anomalous in shape. The F1 waveform does not rise initially as expected, but instead dips below the baseline value before rising above threshold. The waveform then abruptly rises like the other waveforms, but then continues to rise over a much longer timescale. Waveform B2 has the initial fast rise as expected but also continues to have a small rise over a long timescale. Each collected signal equilibrates to nearly the same magnitude by the end of the full window.

Figure 2(b) shows the baseline-corrected waveforms as each begins its motion away from the baseline. This panel shows that each waveform begins its movement away from baseline at a different point in time. This apparent timing difference is due to each channel being individually triggered, causing different signal shapes and amplitudes to result in varying acquisition trigger timing. This inconsistent trigger timing appears to be a significant source of the energy and position distortions subsequently discussed.

The simplest analysis method is to obtain a value for the charge from each signal completely independently. This method is referred to as the individual trigger analysis. The raw waveforms were shifted in time relative to waveform F2 such that each signal reached a threshold of 300 channels at the same time, shown in Figure 2(c). A 300-channel threshold was found to be sufficient to reject noise; the use of waveform F2 as the reference was arbi-

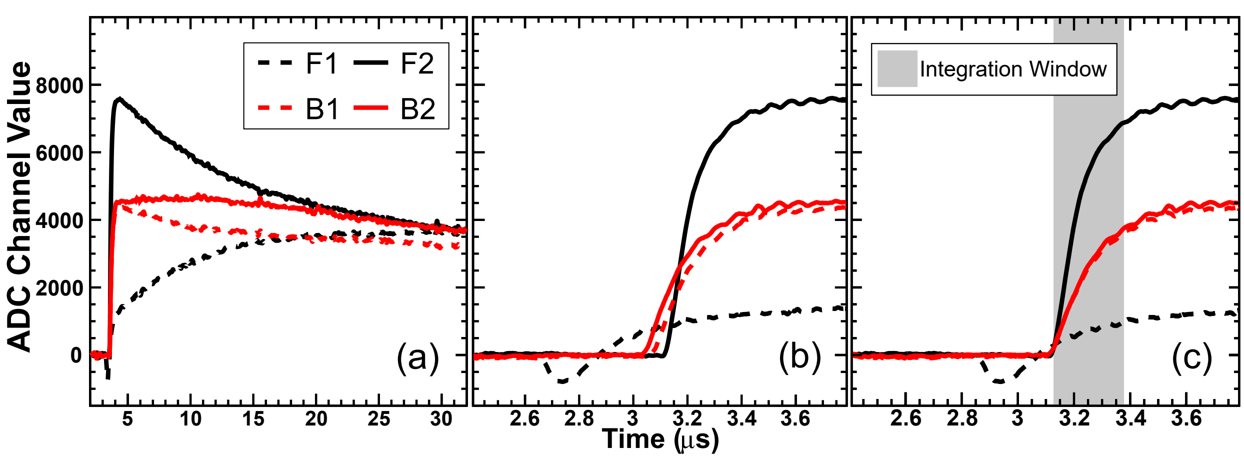

Figure 2: Individual trigger analysis method for waveforms collected by all four contacts for a single incident particle. Waveforms in black correspond to charge collected by the front side of the detector, while waveforms in red (gray) correspond to charge collected by the back side of the detector. (a): Full 32 µs length of baseline-corrected waveforms. (b): Baseline-corrected waveforms over the time the waveforms begins to rise. (c): Individual trigger analysis method: each waveform is shifted in time such that each reaches threshold at the same time and is then integrated over 0.25 µs, as indicated by the gray box.

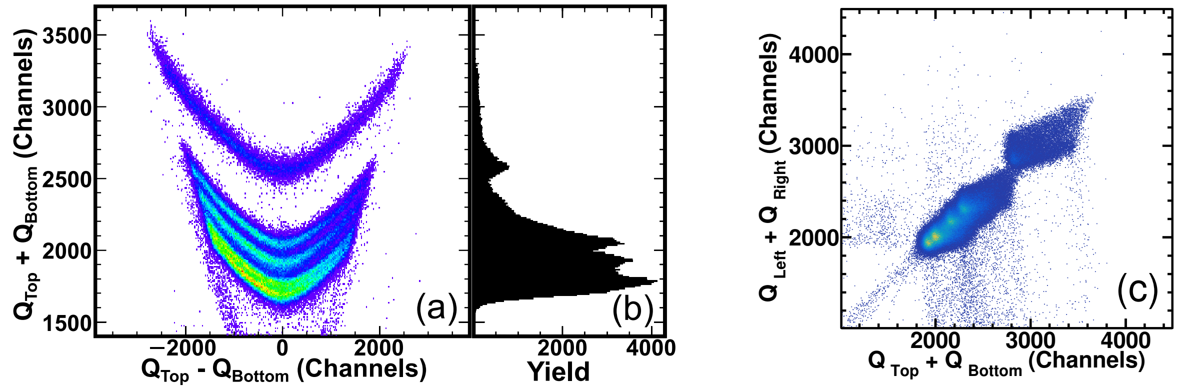

Figure 3: Raw energy versus position spectrum using the individual trigger analysis. Data is from a ^{228}Th alpha source exposed to the full DADL detector surface. (a): The vertical axis is proportional to the total energy deposited. The horizontal axis is related to the vertical position of incidence. (b): Projection of the left panel onto the vertical axis providing an energy spectrum. Note the poor energy resolution obtained using this method. (c): Total charge collected from the back face versus the total charge collected from the front face using ^{228}Th source data for the individual trigger analysis method.

trary but remains consistent through the rest of the paper. To approximate charge values in some way similar to those calculated using shaping amplifiers and peak-sensing ADCs, each signal was integrated over a window of 0.25 µs starting from the time the signal first reached threshold, as shown by the shaded gray area in Figure 2(c).

To investigate the performance of this individual trigger analysis method, alpha particles from a ^{228}Th source were measured. A simple plot was created using the total charge collected by a face (ex. $Q_{\text{Top}} + Q_{\text{Bottom}}$) which represents energy, and the difference in charge collected by the two contacts on the same face ($Q_{\text{Top}} - Q_{\text{Bottom}}$) which represents position and is shown in Figure 3, panel (a). Because the energy deposited by an alpha particle from the source is discrete, horizontal bands are expected in this plot if there is no position dependence of the apparent measured energy. However this figure shows obvious position-dependence by an approximately hyperbolic curvature and an understandably poor energy resolution as evidenced by panel 3(b) which shows the projection onto the vertical axis of panel (a). This feature has been observed and corrected for in previous experiments which used conventional ASICs electronics.The curvature is more severe compared to ref. [5] due to the lack of shaping electronics and the short integration window. Figure 3(c) shows the total charge collected from the back face of the detector as a function of the total charge collected from the front face of the detector for the individual trigger analysis method. Although the data is grossly linear, there is significant spread. The shape of this spread is directly related to the shape of the distributions in panel (a). The severity of this position dependent energy distortion prompted the study of the particle position reconstruction using an alpha beam and a custom brass mask (design shown in Figure 4).

The brass mask was constructed with holes diameters of 1/64, 1/32 and 3/64 inch. The right-angle slits in the mask are 1/32 inch wide. To better evaluate events occurring on the absolute edges of the detector and to calibrate position scaling parameters $c_{x,y}$ in Equations

1 and 2, some of the slits were extended past the physical edge of the detector. The scaling parameters are determined by the ratio $c_x = 1/x_{edge}$. To find x_{edge}, data from the horizontal slit extending past the detector edge was projected onto the X-axis, as shown in Figure 5(a), and fit using the following sigmoid function,

$$f(x) = \frac{a}{1 + e^{(x - x_{edge})/\sigma}}. \quad (6)$$

The midpoint of this sigmoid function is defined to be x_{edge}. An identical treatment is performed using the vertical slit to find y_{edge} and the vertical scaling parameter.

The individual trigger analysis method was used with Equations 1 and 2 to calculate the position of 7.22 MeV/nucleon alpha beam particles incident on the masked DADL detector, as shown in Figure 5(b). This data shows compressed calculated positions near the center edges of the detector and stretched positions near the corners, resulting in a curved "pin cushion" appearance. This curved distortion is most visible on the left side of the position plot where the slit in the mask is straight and vertical. In addition, the width of the slits are not uniform which is most easily seen in the wide bottom of the central vertical slit which narrows near the middle of the detector.

Previous experiments have used a quadratic correction method in order to minimize both energy spectrum curvature and position distortions like those seen in Figures 3 and 5(b), respectively [10]. This correction improves energy resolution significantly, but fails to fully correct for position distortions. An ideal analysis would eliminate the need for an empirical correction while maintaining good resolution.

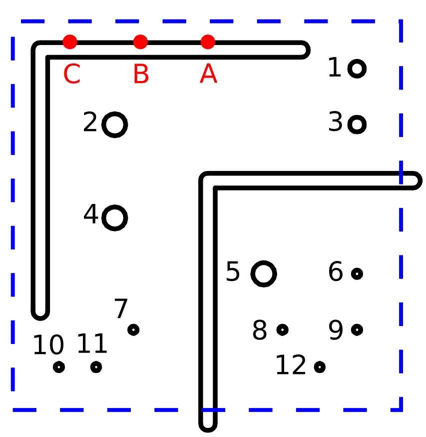

Figure 4: The DADL detector, with edges marked by the dashed box, was positioned behind the mask. Holes in the mask are numbered for reference in Figure 9. Lettered positions along the top horizontal slit indicate positions for waveforms in Figure 10.

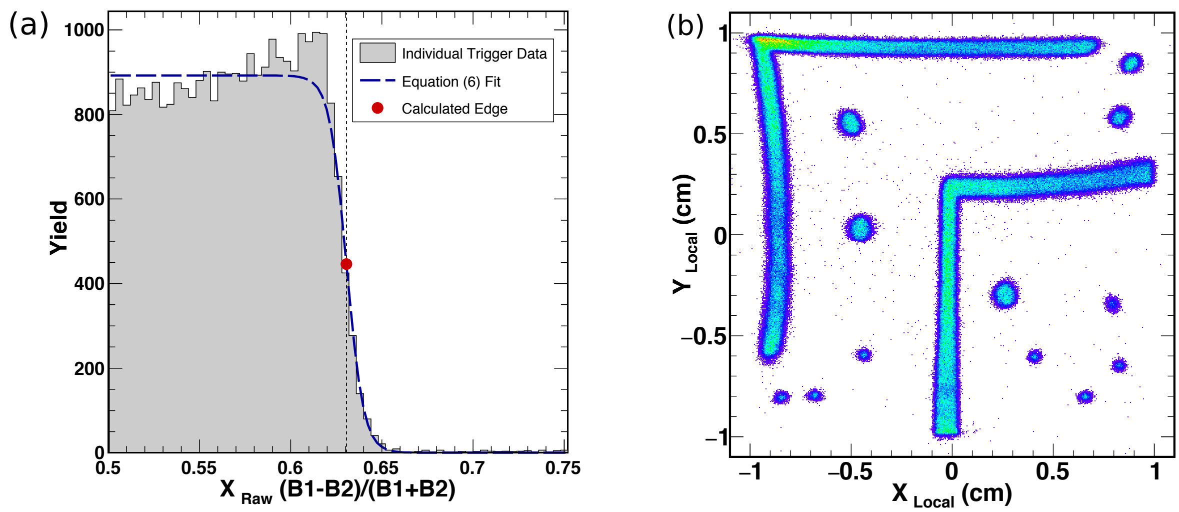

Figure 5: (a): Raw individual trigger data from the middle horizontal slit around 0.25 in Y_{Local} at the detector edge was projected onto the X-axis. This was fit with the sigmoid function shown in Equation 6. The inflection point of this fit was defined as the edge of the detector, or x_{edge}, and used to calculate the scaling parameter. An analogous procedure was completed for the middle vertical slit.

(b): Position plot from 7.22 MeV/nucleon alpha beam using individual trigger analysis method with visible "pin cushion" distortions.

An alternative analysis method was developed that is referred to as the summed trigger analysis method. This method assumes that the distortions in the shape of the individual waveforms F1 and F2 are more severe than the distortions in the sum waveform F1 + F2, and similarly for B1 and B2. To obtain the sum waveform, it was essential for all four waveforms to have the same absolute timing. While the waveform digitizer does not record each waveform with the same absolute time (as seen in Figure 2(a)) it does record a timestamp of the trigger time for each channel. Waveform F2 was again used as the reference point and the other three waveforms were each time-shifted by their respective differences in timestamps. Figure 6(a) shows the same waveforms with the same original timing as in Figure 2(b). Applying the timestamp difference to each waveform results in the waveforms shown in panel 6(b), where all four signals depart from baseline at essentially the same time (no more than a few nanoseconds different).

Once time-corrected, the waveforms from each face were summed (F1+F2 and B1+B2), as shown in Figure 6(c), giving a total charge signal. This signal shape is at least qualitatively consistent with what would be expected from a standard silicon semiconductor detector without resistive electrodes. A threshold was then applied to this summed waveform at 600 channels above baseline. The F1 and F2 individual signals were integrated for a window of 0.250 µs starting 0.600 µs after the F1+F2 sum signal crossed threshold; the B1 and B2 individual signals were integrated for a window of 0.250 µs starting 0.600 µs after the B1+B2 sum signals crossed threshold. This delay in integration was chosen so that integration takes place after all the charge is collected on each electrode and before significant equilibration between the coupled electrodes on a single face occurs. These motivations for the delay in

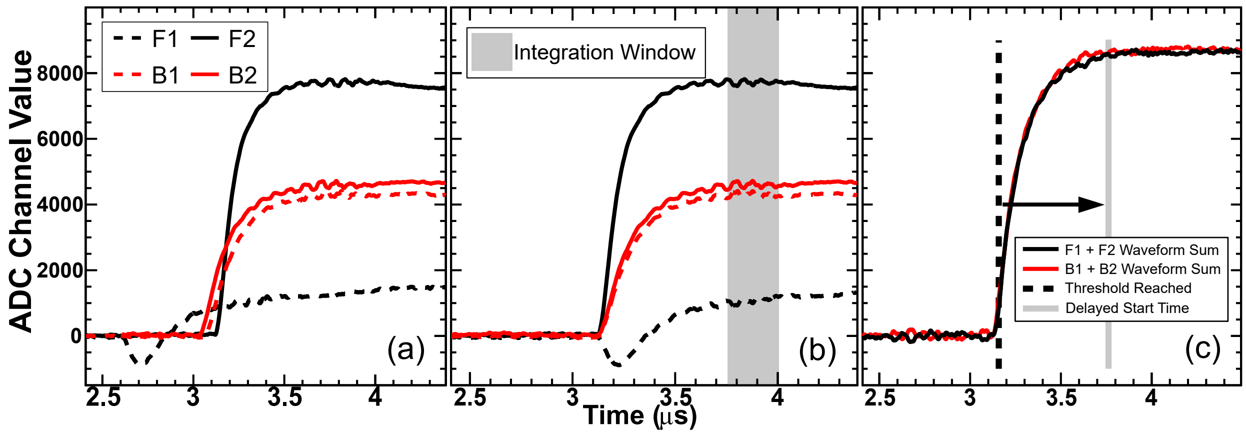

Figure 6: Summed trigger analysis method. (a): Raw waveforms: Baseline-adjusted waveforms from all four contacts for a single incident particle. This panel is identical to Figure 2(b). (b): Time correction: Each waveform is shifted in time based on the time stamp relative to waveform F2. Each waveform is now integrated over 0.25 µs as indicated by the gray box. (c): Time corrected sum: Sums of waveforms collected from detector front (black) and back (red, gray). The dashed line indicates the time the summed waveforms reach threshold and is then delayed by 0.6 µs as indicated by the arrow. This delayed time (gray vertical line) is used as the integration start time for each waveform in panel (b).

integration are further discussed later. These integrated values were recorded and used to calculate position and energy exactly as was done in Figures 3 and 5(b). This integration window is illustrated in Figure 6(b) in gray. The energy-position spectra generated using the summed trigger analysis are shown in Figure 7. These energy spectra lack the position dependent curvature, resulting in an energy resolution of 160 keV FWHM for the 8.8 MeV

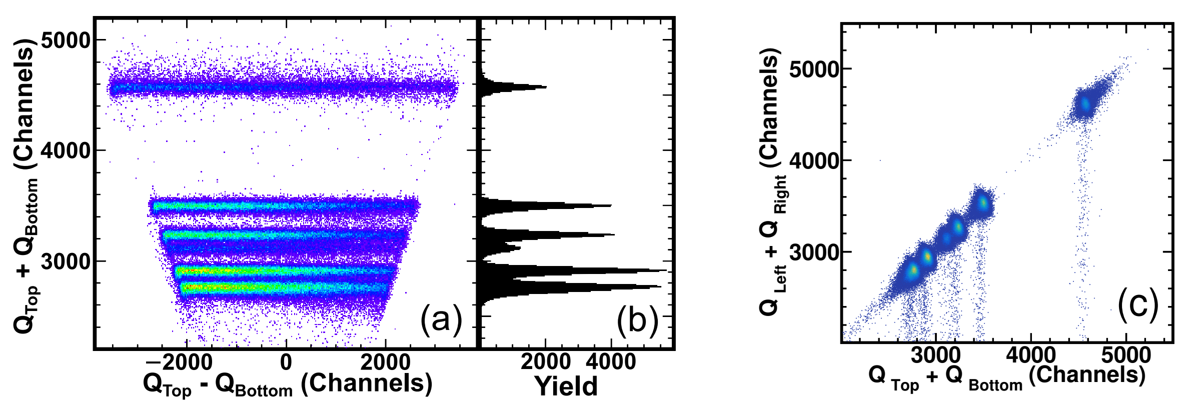

Figure 7: Raw energy versus position plot generated using the summed trigger analysis of individual waveforms. Data is from a ^{228}Th alpha source exposed to the full DADL detector surface. (a): The vertical axis is proportional to the total energy deposited. The horizontal axis is related to the vertical position of incidence. (b): Projection of the left panel onto the vertical axis providing an energy spectrum. Note the lack of curvature with position and improved energy resolution obtained using this method (c): Total charge collected from the back face versus the total charge collected from the front face using ^{228}Th source data for the summed trigger analysis method.

peak, significantly improved as compared to Figure 3. Figure 7(c) shows the total charge collected from the back face of the detector as a function of the total charge collected from the front face of the detector for the summed trigger analysis method. Here, the characteristic spread in data as in Figure 3(c) is largely absent. There is tailing observed below the bulk of data where the back face is missing charge. In a separate experiment, it was determined that these events occur when a particle is incident on or near the back guard ring and as such are excluded from further analysis. Because in this work we have focused primarily on minimizing position distortion, this energy resolution is somewhat poorer than the quadratic correction analysis in ref. [10]. Nevertheless, ongoing work with the summed trigger analysis suggests that it may be possible to adjust the integration parameters to improve this energy resolution while minimizing position distortion. This will be the focus of a future publication.

Analogous to Figure 5(b), the positions of 7.22 MeV/nucleon alpha beam particles incident on the masked DADL detector were calculated using the summed trigger analysis method and are shown in Figure 8. The "pin-cushion" distortion that was present in Figure 5(b) is largely eliminated. The widths of the slits on the mask are also now uniform, with no visible curvature.

Using data from 7.22 MeV/nucleon alpha particle beams impinged directly onto the masked DADL detector, hole-center to hole-center distance measurements for the two analysis methods were compared to the known hole patterns in the mask. The hole center was found by gating on each hole in Figures 5(b) and 8, projecting to the X and Y axes, and taking the mean of a Gaussian fit. Figure 9 shows the difference between the known distances between pairs of holes and the calculated distances between corresponding data from both analysis methods. The ordered pairs in Figure 9 correspond with all combinations of hole pairs as labeled in Figure 4. In almost every case, the accuracy was significantly improved using the summed trigger method. The deviation from mask measurements for the summed trigger method spans a range from −109 µm to 359 µm while the individual trigger method spans a range from −1658 µm to 598 µm.

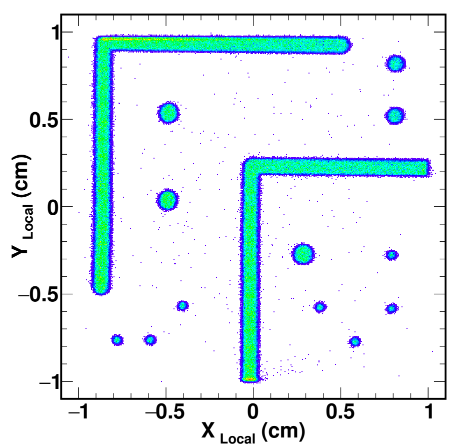

Figure 8: Position plot calculated using the summed trigger analysis method from 7.22 MeV/nucleon alpha beam.

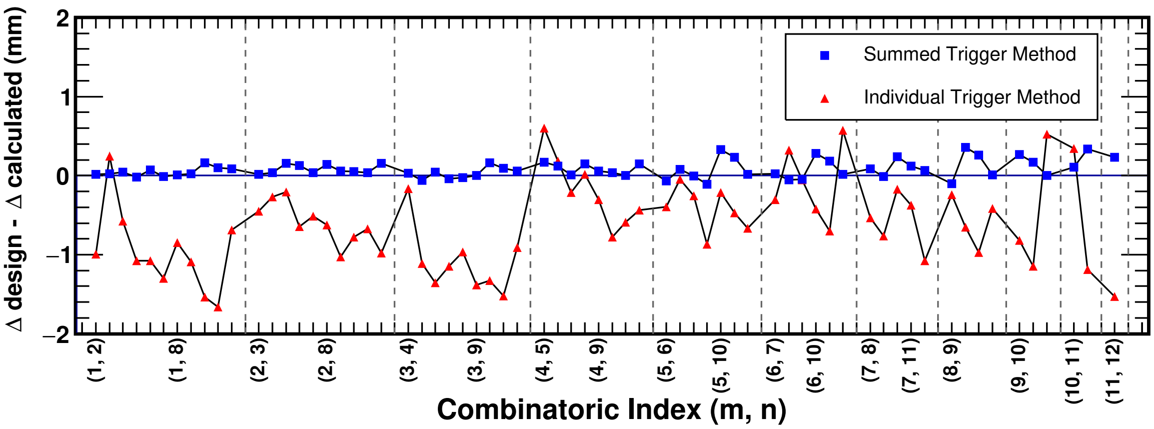

Figure 9: Difference between hole-center to hole-center distances obtained from the mask dimensions and calculated using data from both analysis methods. This distance difference is plotted as a function of a combinatoric index that accounts for every combination of hole pairs. Hole pairs are indicated by (m, n), where m and n correspond with hole number labels from Figure 4. Error is calculated from the mean of the Gaussian fit used to obtain hole center locations and is smaller than the markers.

The delayed integration start time and duration were optimized using three guiding objectives: maximize energy resolution, minimize scaling constants $c_{x,y}$, and minimize position reconstruction distortions by monitoring distance deviations from mask measurements shown in Figure 9. When the integration window started at the initial summed threshold indicated by the dashed line in Figure 6(c), severe position and energy distortions were still obtained. The integration of the negative portion of the bimodal signal (i.e. waveform F1 in Figure 6) yields a negative value, resulting in the magnitude of the calculated X or Y value being greater than the known upper limit of 1 from the size of the detector. This permits particles incident near the edge to have calculated positions outside the active area of the detector, yielding a “barrel” distortion opposite in nature to that shown in Figure 5(b). The barrel distortions were found to disappear with a 0.6 µs delay, effectively starting integration directly after the initial fast rise of the summed waveform. Longer delays and greater integration lengths give larger scaling constants and worse energy resolution due to the waveforms approaching the same value over a long period of time. It was determined that only a small fraction of the waveform was necessary to obtain small scaling factors and excellent resolution.

Examination of individual waveforms demonstrates a position dependence in the shape of the signal shown in Figure 10. Each panel in this figure shows waveforms collected by all four contacts at three different positions on the masked DADL detector. These locations are located across the top of the detector and correspond to positions lettered in Figure 4. For signals originating from particles incident far away from a contact, such as waveform F1 in Figure 10(A), the waveform is bimodal, dipping below baseline followed by a slow rise.

Signals collected by contacts close to the incident particles, such as waveform F2 in Figure 10(A), or even midway between the contacts, such as waveforms B1 and B2 in 10(A), show an expected pulse shape typical of silicon detectors, with a fast initial rise and then a gradual

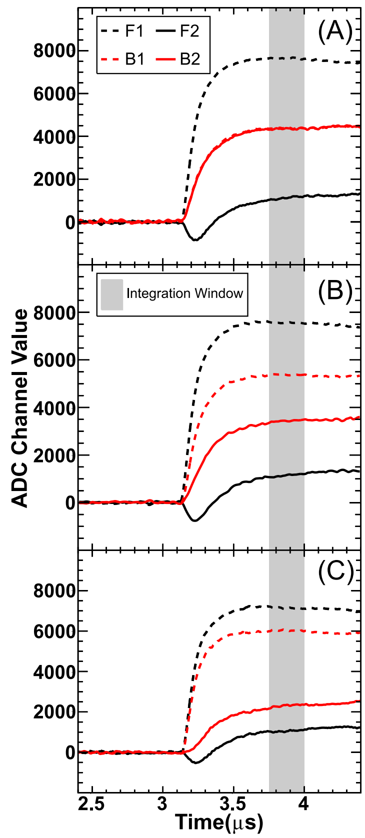

Figure 10: Waveforms collected at all four contacts from incident 7.22 MeV/nucleon alpha particles. All particles are incident near the very top of the detector. The top panel represents a hit near the center (horizontally) of the detector as illustrated by position A in Figure 4. The center and bottom panels represent hits moving progressively toward the upper left corner of the detector as represented by positions B and C, respectively.

decay. Figure 10(B) shows waveforms from a position closer to the corner than panel (A); panel (B) is closest to the corner. Waveform F1 shows qualitatively the same behavior in each case, dipping negative before rising. As the position is moved closer to the corner waveform B2 becomes more like F2. This waveform behavior when a particle is incident near a contact occurs for every contact.

The shape of the waveform for a given contact evolves gradually, becoming more distorted for larger distances between the position of the ionization and the contact. The distortion seen is an increasingly negative initial pulse before the expected rise, and a hindered rise. This behavior can be understood as arising from the capacitive coupling of the two resistive faces of the detector [11]. In this work, it was found that there exist position dependent capacitively induced currents, which can result in bimodal pulses. The propagation of charge across one resistive face is capacitively coupled to the other face, and thus there is a "settling time" determined by the capacitance of the detector and the resistances relevant for any particular position. Since the distortions are most severe near the edges, the waveforms with the smallest amplitude are the most affected. However, when the particle is incident near two edges as in Figure 10(C), the negative component of the bimodal feature in F2 is reduced and is absent in B2. It is thought that as opposite charges are collected off of each face of the detector at roughly the same time, the induced current effects begins to cancel. Nevertheless, though conventional shaping amplifiers can be used, shaping a signal with a large component of the wrong polarity and with a long time before settling to the correct polarity leads to significant under-measurement of the true charge. The summed trigger analysis method outlined here avoids these distortions by waiting for the settling time of the detector and measuring the charge on all contacts over the same time interval. In this way, good energy resolution and good position resolution are obtained without the need for empirical corrections.

5. Summary

The DADL detector has previously shown position and energy non-linearities that require empirical correction methods in order to compensate for the distortions of the pulse shape near the detector edges and retain the good intrinsic position resolution and energy resolution. In this work, the position and energy resolutions of two novel waveform analysis methods for this detector have been characterized. The individual trigger method that treats each waveform using a threshold and short integration window yielded non-linearities. These non-linearities are qualitatively similar in nature to those observed with conventional shaping electronics, though much larger in magnitude with the individual trigger method. These non-linearities are due to the distortion of the waveforms arising from the capacitive coupling of the two resistive surfaces of the detector. As a result, a new summed trigger analysis method has been developed that uses a region of the waveforms that is free from the distortions. This method preserves the excellent position and energy resolution intrinsic to the silicon detector.

6. Acknowledgements

Supported by the following: National Science Foundation Research Experiences for Undergraduates Grant PHY-1659847 & Welch Foundation Grant A-1266 & Department of Energy Grant DE-FG02-93ER40773 & Department of Energy, National Nuclear Security Administration Grant DE-NA0003841. We would like to thank the staff of the Cyclotron Institute for providing excellent beams.

References

[1] S. Aiello, Chimera: a project of a 4π detector for heavy ion reactions studies at intermediate energy, Nucl. Phys. A 583 (1995) 461.

[2] J. Pouthas, INDRA, a 4π charged product detection array at GANIL, Nucl. Instr. and Meth. A 357 (1995) 418.

[3] B. Davin et al., LASSA: a large area silicon strip array for isotopic identification of charged particles, Nucl. Instr. and Meth. A 473 (2001) 302.

[4] M.S. Wallace et al., The high resolution array (HiRA) for rare isotope beam experiments, Nucl. Instr. and Meth. A 583 (2007) 302.

[5] L.A. McIntosh et al., Performance of position-sensitive resistive silicon detectors in the Forward Array Using Silicon Technology (FAUST), Nucl. Instr. and Meth. A (2020).

[6] S.N. Soisson et al., A dual-axis dual-lateral position-sensitive detector for charged particle detection, Nucl. Instr. and Meth. A 613 (2010) 240.

[7] R. Loveza et al., A novel Calorimeter Telescope for identification of relativistic heavy-ion reaction channels, Nucl. Instr. and Meth. A 562 (2006) 298.

[8] 1 Royal Buildings, Lancing, Business Park, West Sussex, BN15 8SJ, UK, Micron Semiconductor Ltd., http://www.micronsemiconductor.co.uk, 2020.

[9] G.L. Engel et al., A multi-channel integrated circuit for use in low- and intermediate-energy nuclear physics—HINP16C, Nucl. Instr. and Meth. A 573 (2007) 418.

[10] L.A. Heilborn, Proton-Proton Correlation Functions Measured Using Position-Sensitive FAUST, Ph.D. thesis, Texas A&M University, 2018.

[11] M. C. Solal, The origin of duo-lateral position-sensitive detector distortions, Nucl. Instr. and Meth. A 572 (2007) 1047.